

# Femtoscopy can tell whether $Z_c(3900)$ and $Z_{cs}(3985)$ are resonances or virtual states

Zhi-Wei Liu,<sup>1</sup> Jun-Xu Lu,<sup>1</sup> Ming-Zhu Liu,<sup>2,3</sup> and Li-Sheng Geng<sup>1,4,5,6,\*</sup>

<sup>1</sup>School of Physics, Beihang University, Beijing 102206, China

<sup>2</sup>Frontiers Science Center for Rare Isotopes, Lanzhou University, Lanzhou 730000, China

<sup>3</sup>School of Nuclear Science and Technology, Lanzhou University, Lanzhou 730000, China

<sup>4</sup>Peng Huanwu Collaborative Center for Research and Education, Beihang University, Beijing 100191, China

<sup>5</sup>Beijing Key Laboratory of Advanced Nuclear Materials and Physics, Beihang University, Beijing 102206, China

<sup>6</sup>Southern Center for Nuclear-Science Theory (SCNT), Institute of Modern Physics, Chinese Academy of Sciences, Huizhou 516000, China

There have been extended and heated discussions on the nature of the two exotic states,  $Z_c(3900)$  and  $Z_{cs}(3985)$ , particularly whether they are resonances or virtual states. We demonstrate for the first time that the femtoscopic technique can be used to unambiguously distinguish between such two scenarios. More concretely, we show that the  $D^0 D^{*-}/D^0 D_s^{*-}$  correlation functions are significantly different in the high-momentum region, especially in small collision systems of the order of 1 fm, as produced in pp collisions at the LHC, which can unambiguously tell whether  $Z_c(3900)/Z_{cs}(3985)$  is a resonant or a virtual state. For the  $Z_{cs}(3985)$ , the  $D^0 D_s^{*-}$  results at zero momentum are significantly different in the two scenarios. We hope all these discoveries can stimulate further experimental studies and help clarify the nature of the many exotic states discovered.

**Introduction.**—In 2013, the BESIII Collaboration and Belle Collaboration observed a hidden-charm tetraquark candidate  $Z_c^\pm(3900)$  in the  $J/\psi\pi^\pm$  invariant mass distribution of the  $e^+e^- \rightarrow J/\psi\pi^+\pi^-$  process [1, 2]. This charged charmoniumlike state was subsequently confirmed by the CLEO-c Collaboration in the  $e^+e^-$  annihilation process [3] and the semi-inclusive decays of  $b$ -hadrons at the D0 experiment [4]. In 2020, the BESIII Collaboration reported the first signal of a hidden-charm state with strangeness,  $Z_{cs}^-(3985)$ , in the  $K^+$  recoil-mass spectrum of the  $e^+e^- \rightarrow K^+(D^{*0}D_s^- + D^0D_s^{*-})$  reaction [5]. Since the quark contents of the charged  $Z_c^-(3900)/Z_c^+(3900)$  and  $Z_{cs}^-(3985)$  states are  $c\bar{c}d\bar{u}/c\bar{c}u\bar{d}$  and  $c\bar{c}s\bar{u}$ , respectively, the latter is often interpreted as the strangeness partner of the former in terms of the SU(3)-flavor symmetry. We note that their isospin quantum numbers have been fixed by the discovery of their neutral partners [6, 7].

There have been extensive studies on the nature of the  $Z_c(3900)/Z_{cs}(3985)$  states, treating them as hadronic molecules of  $D^0 D^{*-}/D^0 D_s^{*-}$  [8–11], compact tetraquark states [12–14], and threshold effects [15–19](see Refs. [20–26] for recent reviews), but no firm conclusion has been reached. Especially, due to the lack of reliable theoretical understanding of the  $D^0 D^{*-}$  and  $D^0 D_s^{*-}$  interactions, there have been long and heated discussions on whether  $Z_c(3900)$  and  $Z_{cs}(3985)$  are resonances or virtual states. In experimental analyses based on the Breit-Wigner parametrization,  $Z_c(3900)$  and  $Z_{cs}(3985)$  are suggested to be typical resonances [1, 2, 5]. However, various theoretical re-analyses of the same data suggest they can be either resonances or virtual states [27–30].

In recent years, femtoscopy, which measures two-hadron momentum correlation functions (CFs) in high-energy collisions, has made remarkable progress in revealing the dynamics of the strong interactions between pairs of stable and unstable hadrons [31–33]. Thanks to the abundant rare hadrons produced and the various particle emission sources available in

relativistic pp, pA, and AA collisions, the femtoscopic technique can be used, not only to study the strong interactions involving unstable hadrons that are difficult or impossible in traditional scattering experiments, but also to provide more and complementary information compared with the measurement of invariant mass distributions. A lot has been learned about the meson-meson [34–38], meson-baryon [39–43], and (anti)baryon-(anti)baryon [44–56] interactions in the light quark (u, d, s) sector with the femtoscopic technique. More recently, the successful measurements of the  $\bar{D}N$ ,  $D^{(*)}\pi$ , and  $D^{(*)}K$  CFs demonstrated the huge potential to access the charm sector experimentally [57, 58]. With the upgraded ALICE apparatus and the larger data sample size expected at LHC run 3, 4, and 5, more reactions can be accessed with high precision in the future [59].

On the other hand, the experimental studies have also triggered a large number of theoretical studies [60–72], especially in the charm and bottom sectors [73–84]. It was shown that femtoscopy offers a valuable means to directly test the hadronic molecular picture of the exotic hadrons [75–78]. However, it is worth noting that the above studies mainly focus on bound states, with little discussion about resonant or virtual states. In this work, we show how one can utilize the femtoscopic technique to study hadronic interactions in the presence of virtual or resonant states. In particular, assuming that  $Z_c(3900)/Z_{cs}(3985)$  is a molecular state of  $D^0 D^{*-}/D^0 D_s^{*-}$ , one can distinguish whether  $Z_c(3900)/Z_{cs}(3985)$  is a resonant or a virtual state by measuring the  $D^0 D^{*-}/D^0 D_s^{*-}$  CFs.

*Model-independent formulations of the  $D^0 D^{*-}/D^0 D_s^{*-}$  interactions and corresponding correlation functions.*—We first explain how to describe the  $D^0 D^{*-}/D^0 D_s^{*-}$  interactions model independently and calculate the femtoscopic CFs. Since the  $D\bar{D}^*$  and  $D\bar{D}_s^*$  thresholds are 400 – 600 MeV above the corresponding  $J/\psi\pi$  and  $J/\psi\bar{K}$  thresholds, coupled-channel effects on the CFs can be safely neglected. From the point of view of effective field theories (EFTs), the lowest order  $D^0 D^{*-}/D^0 D_s^{*-}$  interactions can be described by a constant contact-range potential without deriva-

\* Corresponding author: lisheng.geng@buaa.edu.cn

tives [8, 27, 85, 86], which, however, can only generate a bound or virtual state below the respective thresholds. To produce a resonant state above the thresholds, it is necessary to introduce energy dependence to the leading-order potential [8, 27, 87]. Thus, the most general potential up to the next-to-leading order has the following form

$$V(k) = a + b k^2, \quad (1)$$

where  $k = \frac{\sqrt{s-(m_1+m_2)^2}\sqrt{s-(m_1-m_2)^2}}{2\sqrt{s}}$  represents the c.m. momentum of the particle pair, and  $a$  and  $b$  are (real) low-energy constants (LECs) to be determined. Then, the single-channel  $T$ -matrix can be obtained as

$$T(\sqrt{s}) = [1 - VG(\sqrt{s})]^{-1}V, \quad (2)$$

where  $\sqrt{s}$  represents the c.m. energy. The loop function (in the first/physical Riemann sheet (RS))  $G(\sqrt{s})$  is regularized by a sharp cutoff  $q_{\max}$  of the order of  $0.8 - 1.2$  GeV,

$$G(\sqrt{s}) = \int_0^{|q| < q_{\max}} \frac{d^3 k'}{(2\pi)^3} \frac{E_1(k') + E_2(k')}{2E_1(k')E_2(k')} \times \frac{1}{\sqrt{s^2 - [E_1(k') + E_2(k')]^2 + i\varepsilon}}, \quad (3)$$

with  $E_i(k') = \sqrt{m_i^2 + k'^2}$ . Here, the virtual and resonant states are identified as poles in the second/unphysical RS of the  $T$ -matrix on the real axis below the threshold and in the complex  $s$  plane. For a resonance, the real and imaginary parts of the pole position define its mass and half-width. The loop function in the second/unphysical RS,  $G^{II}$ , is related to that in the first RS, by an analytic continuation as  $G^{II}(\sqrt{s}) = G^I(\sqrt{s}) + ik/(4\pi\sqrt{s})$  with  $\text{Im } k > 0$  [88]. In addition, it is worth calculating the scattering length  $a_0$  and effective range  $r_{\text{eff}}$ , which are defined from the Quantum Mechanics amplitude  $f(k)$  in the effective range expansion around the threshold  $\sqrt{s_{\text{th}}} = m_1 + m_2$ , i.e.,  $f(k) \approx (-1/a_0 + r_{\text{eff}}k^2/2 - ik)^{-1}$ . Thus, we can determine  $a_0$  and  $r_{\text{eff}}$  as [78]

$$-\frac{1}{a_0} = [-8\pi\sqrt{s}T(\sqrt{s})^{-1}]_{\sqrt{s}=\sqrt{s_{\text{th}}}}, \quad (4a)$$

$$r_{\text{eff}} = \left[ \frac{\partial^2}{\partial k^2} (-8\pi\sqrt{s}T(\sqrt{s})^{-1} + ik) \right]_{\sqrt{s}=\sqrt{s_{\text{th}}}}. \quad (4b)$$

According to the Koonin-Pratt (KP) formula [89–91], the femtoscopic CF depends on two quantities, namely,  $\psi$  the scattering wave function of the relative motion for the pair of interest and  $S_{12}$  the particle-emitting source created in relativistic  $pp$ ,  $pA$ , and  $AA$  collisions. The former contains the information on the final-state interaction we are interested in. In general, there are two ways to obtain the scattering wave function, either by solving the Schrödinger equation in coordinate space [92, 93] or the Lippmann-Schwinger (Bethe-Salpeter) equation in momentum space [75, 94]. In this work, since the potential of Eq. (1) is constructed in momentum space, it is convenient first to obtain the reaction amplitude  $T$ -matrix by solving Eq. (2) and then derive the scattering wave function using the relation  $|\psi\rangle = |\varphi\rangle + GT|\varphi\rangle$ , where  $G$  and  $|\varphi\rangle$

represent the free propagator and the free wave function. For the particle-emitting source, we adopt a common static and spherical Gaussian source characterized by a single parameter  $R$ , i.e.,  $S_{12}(r) = \exp[-r^2/(4R^2)]/(2\sqrt{\pi}R)^3$ . We note that past studies showed that the qualitative features of CFs are not sensitive to different parameterizations of the emitting source (see, e.g., Refs. [69, 95]). With the above-specified ingredients and following the formalism of Refs. [77, 78], the CF can be expressed as

$$C(k) = 1 + \int_0^\infty 4\pi r^2 dr S_{12}(r) \theta(q_{\max} - k) \times \left[ |j_0(kr) + T(\sqrt{s}) \tilde{G}(r, \sqrt{s})|^2 - |j_0(kr)|^2 \right], \quad (5)$$

where  $j_0$  is the spherical Bessel function for  $l = 0$ , and the factor  $\theta(q_{\max} - k)$  only operates in the high-momentum region where the CF equals unity. The quantity  $\tilde{G}$  is given by

$$\tilde{G}(r, \sqrt{s}) = \int_0^{|q| < q_{\max}} \frac{d^3 k'}{(2\pi)^3} \frac{E_1(k') + E_2(k')}{2E_1(k')E_2(k')} \times \frac{j_0(k'r)}{\sqrt{s^2 - [E_1(k') + E_2(k')]^2 + i\varepsilon}}. \quad (6)$$

As mentioned above,  $a$ ,  $b$ , and  $q_{\max}$  are the only unknown parameters in describing the  $D^0 D^{*-}/D^0 D_s^{*-}$  interaction. They can be determined by reproducing the pole positions of  $Z_c(3900)$  and  $Z_{cs}(3985)$  in the two scenarios, namely, resonant [96] or virtual [27]. The masses and widths of the  $Z_c(3900)$  and  $Z_{cs}(3985)$  states, as either resonances or virtual states, determined in Refs. [27, 96], the  $D^0 D^{*-}$  and  $D^0 D_s^{*-}$  thresholds, as well as the corresponding parameters  $a$  and  $b$  are listed in Table I. In addition, we also calculate the scattering length and effective range that characterize the  $D^0 D^{*-}/D^0 D_s^{*-}$  interaction.

*Results and discussions.*—We present the  $D^0 D^{*-}$  CF for three typical source sizes  $R = 1, 2$ , and  $5$  fm in Fig. 1, where the left (right) panel corresponds to the results obtained with the energy-dependent (constant contact-range) potential, which interprets the  $Z_c(3900)$  as a resonant (virtual) state. The bands reflect the sharp cutoff variation in the  $q_{\max} = 0.8 - 1.2$  GeV. In the virtual state scenario, the  $D^0 D^{*-}$  CF is enhanced (compared to unity) in a wide range of the relative momentum  $k$ , which is similar to the result obtained with a weakly attractive potential in the square-well model [75]; but in the resonant state scenario, although the  $D^0 D^{*-}$  CF is still enhanced in the low-momentum region, it is suppressed (compared to unity) in the high-momentum region<sup>1</sup> and exhibits a minimum, which is the key to distinguishing between the two scenarios. As the source size  $R$  decreases, the difference in the CFs between these two scenarios becomes more

<sup>1</sup> The high-momentum region refers to the range  $k \gtrsim k_R$ , where  $k_R$  is the c.m. momentum corresponding to the resonance mass. Here, the  $k_R$  associated with  $Z_c(3900)$  and  $Z_{cs}(3985)$  are 152 and 147 MeV/c in the c.m. frame of  $D^0 D^{*-}$  and  $D^0 D_s^{*-}$ , respectively.

TABLE I. Masses and widths of  $Z_c(3900)$  and  $Z_{cs}(3985)$  obtained experimentally [96] and in the theoretical work of Ref. [27], the  $D^0 D^{*-}$  and  $D^0 D_s^{*-}$  thresholds, the values of the parameters  $a$  and  $b$ , the scattering length  $a_0$  and effective range  $r_{\text{eff}}$ . The sharp cutoff  $q_{\text{max}}$  is fixed at 1 GeV.

	Scenario	$M$ [MeV]	$\Gamma$ [MeV]	$m_1 + m_2$ [MeV]	$a$	$b$ [MeV $^{-2}$ ]	$a_0$ [fm]	$r_{\text{eff}}$ [fm]
$Z_c(3900)$	Res. [96]	3887.1	28.4	$D^0 D^{*-}$ (3875.1)	-101.68	-1380.60	-0.57	-4.83
	Vir. [27]	3796	0	$D^0 D^{*-}$ (3875.1)	-87.36	0	-0.39	0.31
$Z_{cs}(3985)$	Res. [96]	3988	13	$D^0 D_s^{*-}$ (3977.04)	-84.17	-2894.16	-0.34	-15.80
	Vir. [27]	3967	0	$D^0 D_s^{*-}$ (3977.04)	-130.21	0	-1.27	0.29

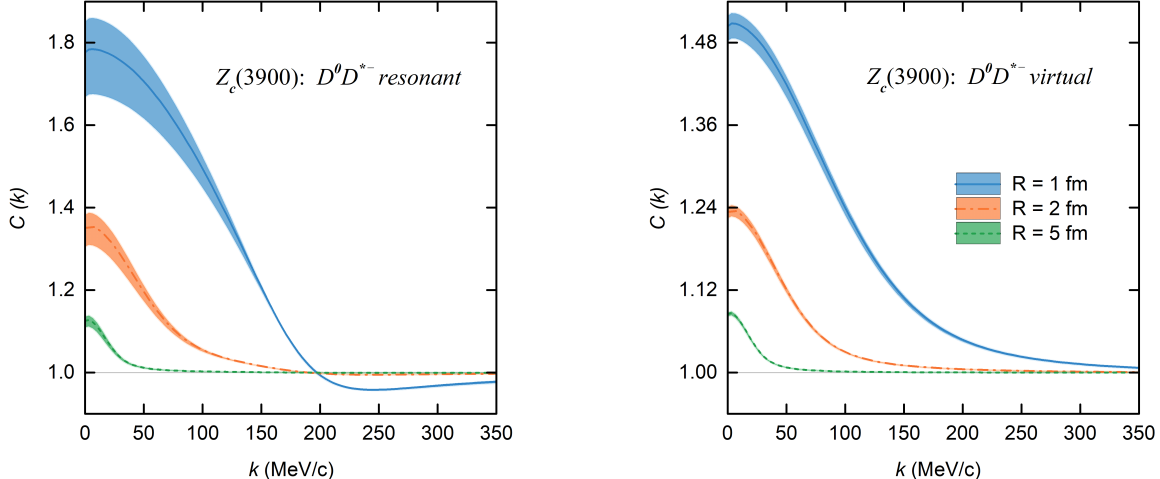


FIG. 1.  $D^0 D^{*-}$  correlation function as a function of the relative momentum  $k$  for different source sizes  $R = 1, 2$ , and  $5$  fm. The results are obtained with the energy-dependent potential, which describes the  $Z_c(3900)$  as a resonant state (left panel), and with the constant contact-range potential, which interprets the  $Z_c(3900)$  as a virtual state (right panel), respectively. The bands reflect the variation of the sharp cutoff in the range of  $q_{\text{max}} = 0.8 - 1.2$  GeV, where the corresponding parameters  $a$  and  $b$  are redetermined by reproducing the pole position listed in Table I.

significant, which can be attributed to the short-range nature of the strong interaction. In addition, we note that the  $D^0 D^{*-}$  CFs in different scenarios are close to each other at zero momentum, which is consistent with the fact that their scattering lengths (shown in Table I) are similar.

The  $D^0 D_s^{*-}$  CFs are shown in Fig. 2. As expected, due to the SU(3) light-flavor symmetry, the  $D^0 D_s^{*-}$  CFs exhibit similar behaviors as the  $D^0 D^{*-}$  CFs discussed above. However, in the resonant state scenario, the suppression in the high-momentum region becomes more significant, which can be attributed to the narrower width of  $Z_{cs}(3985)$ . This is understandable because as the pole approaches the real axis, the influence of the resonant structure on physical observables intensifies. A comprehensive discussion on the influence of the pole positions of virtual or resonant states on the corresponding CFs is presented in the Supplemental Material. Moreover, it is found that the  $D^0 D_s^{*-}$  CFs in the virtual state scenario are significantly larger than those in the resonant case at zero momentum. The scattering length of the former is much smaller than that of the latter. This distinction indicates that the interaction responsible for the virtual state at the threshold is more attractive, providing another feature for distinguishing

whether  $Z_{cs}(3985)$  is a resonant or virtual state.

We emphasize that it is experimentally feasible to distinguish whether  $Z_c(3900)/Z_{cs}(3985)$  is a resonant or virtual state by measuring the  $D^0 D^{*-}/D^0 D_s^{*-}$  CFs, especially in  $pp$  collisions. This is because, on the one hand, the statistical uncertainties of experimental measurements in the high-momentum region are usually much smaller than those in the low-momentum region (see, e.g., Refs [34–58]). On the other hand, our results show that for the  $D^0 D^{*-}$  and  $D^0 D_s^{*-}$  CFs with  $R = 1$  fm, the differences in the CFs between the two scenarios can be as significant as about 0.07 and 0.16 at  $k \approx 230$  and  $k \approx 180$  MeV/c, respectively, and the  $D^0 D_s^{*-}$  results at zero momentum can also provide distinctive information. In addition, a combined analysis of the  $D^0 D^{*-}$  and  $D^0 D_s^{*-}$  CFs will provide a non-trivial test of not only their interactions but also the SU(3) flavor symmetry and its breaking.

*Summary and outlook.*—In this letter, we proposed to decipher the nature of  $Z_c(3900)$  and  $Z_{cs}(3985)$  with the femtoscopic technique. We first evaluated the  $D^0 D^{*-}/D^0 D_s^{*-}$  interactions by reproducing the pole positions of  $Z_c(3900)/Z_{cs}(3985)$  in the resonant and virtual state

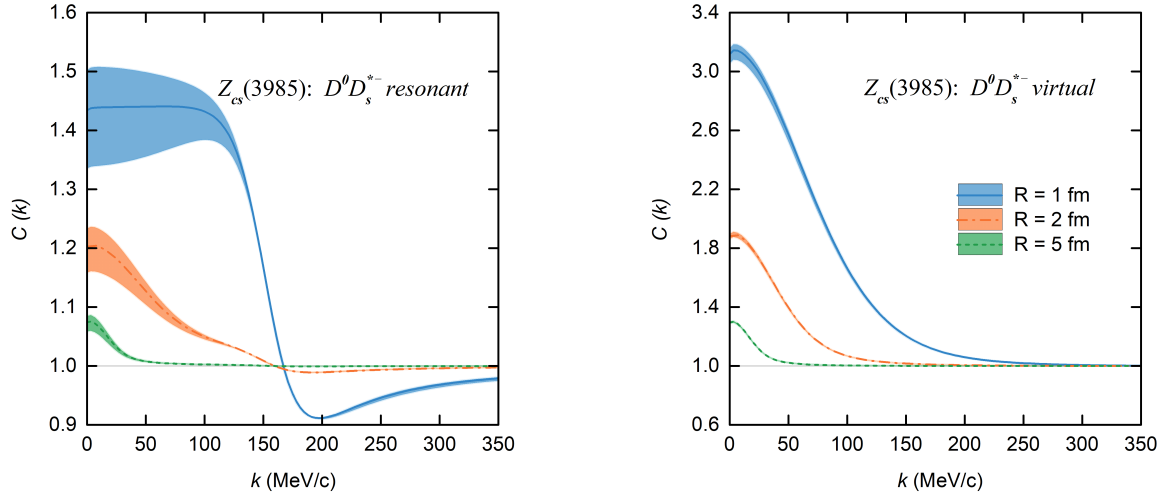


FIG. 2.  $D^0 D_s^{*-}$  correlation functions as a function of the relative momentum  $k$  for different source sizes  $R = 1, 2$ , and  $5$  fm. The results are obtained with the energy-dependent potential, which describes the  $Z_{cs}(3985)$  as a resonant state (left panel), and with the constant contact-range potential, which interprets the  $Z_{cs}(3985)$  as a virtual state (right panel), respectively. The bands reflect the variation of the sharp cutoff in the range of  $q_{\max} = 0.8 - 1.2$  GeV, where the corresponding parameters  $a$  and  $b$  are redetermined by reproducing the pole position listed in Table I.

scenarios, respectively, and then calculated the corresponding  $D^0 D_s^{*-}/D^0 D_s^{*-}$  correlation functions. The results show that the  $D^0 D_s^{*-}/D^0 D_s^{*-}$  correlation functions in the high-momentum region are suppressed in the resonant state scenario but enhanced in the virtual state scenario, especially in  $pp$  collisions, which is the key to distinguishing whether  $Z_c(3900)/Z_{cs}(3985)$  is a resonant or a virtual state. In addition, the different  $D^0 D_s^{*-}$  results at zero momentum can also be used to distinguish these two scenarios for the  $Z_{cs}(3985)$  state. Considering experimental precision achievable at present, we strongly encourage our experimental colleagues to measure the  $D^0 D_s^{*-}/D^0 D_s^{*-}$  correlation functions.

It is important to note that the proposed method is model-

independent, which results from the general features of femtoscopic correlation functions and can be applied to clarify the nature of other similar exotic states, such as  $Z_c(4020)$ ,  $Z_b(10610)$ , and  $Z_b(10650)$ .

*Acknowledgments.* We thank Eulogio Oset for a careful reading of the present manuscript. This work is partly supported by the National Key R&D Program of China under Grant No. 2023YFA1606700. Zhi-Wei Liu acknowledges support from the National Natural Science Foundation of China under Grant No.12347180, China Postdoctoral Science Foundation under Grant No.2023M740189, and the Postdoctoral Fellowship Program of CPSF under Grant No.GZC20233381.

- 
- [1] M. Ablikim *et al.* (BESIII), *Phys. Rev. Lett.* **110**, 252001 (2013), arXiv:1303.5949 [hep-ex].
  - [2] Z. Q. Liu *et al.* (Belle), *Phys. Rev. Lett.* **110**, 252002 (2013), [Erratum: Phys.Rev.Lett. 111, 019901 (2013)], arXiv:1304.0121 [hep-ex].
  - [3] T. Xiao, S. Dobbs, A. Tomaradze, and K. K. Seth, *Phys. Lett. B* **727**, 366 (2013), arXiv:1304.3036 [hep-ex].
  - [4] V. M. Abazov *et al.* (D0), *Phys. Rev. D* **98**, 052010 (2018), arXiv:1807.00183 [hep-ex].
  - [5] M. Ablikim *et al.* (BESIII), *Phys. Rev. Lett.* **126**, 102001 (2021), arXiv:2011.07855 [hep-ex].
  - [6] M. Ablikim *et al.* (BESIII), *Phys. Rev. Lett.* **115**, 112003 (2015), arXiv:1506.06018 [hep-ex].
  - [7] M. Ablikim *et al.* (BESIII), *Phys. Rev. Lett.* **129**, 112003 (2022), arXiv:2204.13703 [hep-ex].
  - [8] Z. Yang, X. Cao, F.-K. Guo, J. Nieves, and M. P. Valderrama, *Phys. Rev. D* **103**, 074029 (2021), arXiv:2011.08725 [hep-ph].
  - [9] L. Meng, B. Wang, and S.-L. Zhu, *Phys. Rev. D* **102**, 111502 (2020), arXiv:2011.08656 [hep-ph].
  - [10] V. Baru, E. Epelbaum, A. A. Filin, C. Hanhart, and A. V. Nefediev, *Phys. Rev. D* **105**, 034014 (2022), arXiv:2110.00398 [hep-ph].
  - [11] M.-J. Yan, F.-Z. Peng, M. Sánchez Sánchez, and M. Pavon Valderrama, *Phys. Rev. D* **104**, 114025 (2021), arXiv:2102.13058 [hep-ph].
  - [12] Z.-G. Wang, *Chin. Phys. C* **45**, 073107 (2021), arXiv:2011.10959 [hep-ph].
  - [13] L. Maiani, A. D. Polosa, and V. Riquer, *Sci. Bull.* **66**, 1616 (2021), arXiv:2103.08331 [hep-ph].
  - [14] R.-H. Wu, C.-Y. Wang, C. Meng, Y.-Q. Ma, and K.-T. Chao, (2023), arXiv:2312.14224 [hep-ph].
  - [15] Q. Wang, C. Hanhart, and Q. Zhao, *Phys. Rev. Lett.* **111**, 132003 (2013), arXiv:1303.6355 [hep-ph].
  - [16] D.-Y. Chen, X. Liu, and T. Matsuki, *Phys. Rev. D* **88**, 036008 (2013), arXiv:1304.5845 [hep-ph].
  - [17] J.-Z. Wang, Q.-S. Zhou, X. Liu, and T. Matsuki, *Eur. Phys. J. C* **81**, 51 (2021), arXiv:2011.08628 [hep-ph].
  - [18] N. Ikeda, R. Molina, and E. Oset, *Phys. Lett. B* **814**, 136120

- (2021), arXiv:2011.13425 [hep-ph].
- [19] S. Prelovsek, C. B. Lang, L. Leskovec, and D. Mohler, *Phys. Rev. D* **91**, 014504 (2015), arXiv:1405.7623 [hep-lat].
- [20] S. L. Olsen, T. Skwarnicki, and D. Zieminska, *Rev. Mod. Phys.* **90**, 015003 (2018), arXiv:1708.04012 [hep-ph].
- [21] M. Karliner, J. L. Rosner, and T. Skwarnicki, *Ann. Rev. Nucl. Part. Sci.* **68**, 17 (2018), arXiv:1711.10626 [hep-ph].
- [22] C.-Z. Yuan, *Int. J. Mod. Phys. A* **33**, 1830018 (2018), arXiv:1808.01570 [hep-ex].
- [23] Y.-R. Liu, H.-X. Chen, W. Chen, X. Liu, and S.-L. Zhu, *Prog. Part. Nucl. Phys.* **107**, 237 (2019), arXiv:1903.11976 [hep-ph].
- [24] N. Brambilla, S. Eidelman, C. Hanhart, A. Nefediev, C.-P. Shen, C. E. Thomas, A. Vairo, and C.-Z. Yuan, *Phys. Rept.* **873**, 1 (2020), arXiv:1907.07583 [hep-ex].
- [25] F.-K. Guo, X.-H. Liu, and S. Sakai, *Prog. Part. Nucl. Phys.* **112**, 103757 (2020), arXiv:1912.07030 [hep-ph].
- [26] L. Meng, B. Wang, G.-J. Wang, and S.-L. Zhu, *Phys. Rept.* **1019**, 1 (2023), arXiv:2204.08716 [hep-ph].
- [27] M.-L. Du, M. Albaladejo, F.-K. Guo, and J. Nieves, *Phys. Rev. D* **105**, 074018 (2022), arXiv:2201.08253 [hep-ph].
- [28] T. Ji, X.-K. Dong, M. Albaladejo, M.-L. Du, F.-K. Guo, and J. Nieves, *Phys. Rev. D* **106**, 094002 (2022), arXiv:2207.08563 [hep-ph].
- [29] L.-W. Yan, Z.-H. Guo, F.-K. Guo, D.-L. Yao, and Z.-Y. Zhou, *Phys. Rev. D* **109**, 014026 (2024), arXiv:2307.12283 [hep-ph].
- [30] Y.-H. Chen, M.-L. Du, and F.-K. Guo, (2023), arXiv:2310.15965 [hep-ph].
- [31] S. Cho *et al.* (ExHIC), *Prog. Part. Nucl. Phys.* **95**, 279 (2017), arXiv:1702.00486 [nucl-th].
- [32] L. Fabbietti, V. Mantovani Sarti, and O. Vazquez Doce, *Ann. Rev. Nucl. Part. Sci.* **71**, 377 (2021), arXiv:2012.09806 [nucl-ex].
- [33] M.-Z. Liu, Y.-W. Pan, Z.-W. Liu, T.-W. Wu, J.-X. Lu, and L.-S. Geng, (2024), arXiv:2404.06399 [hep-ph].
- [34] S. Acharya *et al.* (ALICE), *Phys. Lett. B* **774**, 64 (2017), arXiv:1705.04929 [nucl-ex].
- [35] S. Acharya *et al.* (ALICE), *Phys. Lett. B* **790**, 22 (2019), arXiv:1809.07899 [nucl-ex].
- [36] S. Acharya *et al.* (ALICE), *Phys. Lett. B* **813**, 136030 (2021), arXiv:2007.08315 [nucl-ex].
- [37] S. Acharya *et al.* (ALICE), *Phys. Lett. B* **833**, 137335 (2022), arXiv:2111.06611 [nucl-ex].
- [38] S. Acharya *et al.* (ALICE), (2023), arXiv:2312.12830 [hep-ex].
- [39] S. Acharya *et al.* (ALICE), *Phys. Rev. Lett.* **124**, 092301 (2020), arXiv:1905.13470 [nucl-ex].
- [40] S. Acharya *et al.* (ALICE), *Phys. Rev. C* **103**, 055201 (2021), arXiv:2005.11124 [nucl-ex].
- [41] S. Acharya *et al.* (ALICE), *Phys. Rev. Lett.* **127**, 172301 (2021), arXiv:2105.05578 [nucl-ex].
- [42] S. Acharya *et al.* (ALICE), *Eur. Phys. J. C* **83**, 340 (2023), arXiv:2205.15176 [nucl-ex].
- [43] S. Acharya *et al.* (ALICE), *Phys. Lett. B* **845**, 138145 (2023), arXiv:2305.19093 [nucl-ex].
- [44] L. Adamczyk *et al.* (STAR), *Phys. Rev. Lett.* **114**, 022301 (2015), arXiv:1408.4360 [nucl-ex].
- [45] L. Adamczyk *et al.* (STAR), *Nature* **527**, 345 (2015), arXiv:1507.07158 [nucl-ex].
- [46] J. Adam *et al.* (STAR), *Phys. Lett. B* **790**, 490 (2019), arXiv:1808.02511 [hep-ex].
- [47] M. Isshiki (STAR), *EPJ Web Conf.* **259**, 11015 (2022), arXiv:2109.10953 [nucl-ex].
- [48] S. Acharya *et al.* (ALICE), *Phys. Rev. C* **99**, 024001 (2019), arXiv:1805.12455 [nucl-ex].
- [49] S. Acharya *et al.* (ALICE), *Phys. Lett. B* **797**, 134822 (2019), arXiv:1905.07209 [nucl-ex].
- [50] S. Acharya *et al.* (ALICE), *Phys. Lett. B* **805**, 135419 (2020), arXiv:1910.14407 [nucl-ex].
- [51] S. Acharya *et al.* (ALICE), *Phys. Lett. B* **802**, 135223 (2020), arXiv:1903.06149 [nucl-ex].
- [52] S. Acharya *et al.* (ALICE), *Phys. Rev. Lett.* **123**, 112002 (2019), arXiv:1904.12198 [nucl-ex].
- [53] A. Collaboration *et al.* (ALICE), *Nature* **588**, 232 (2020), [Erratum: Nature 590, E13 (2021)], arXiv:2005.11495 [nucl-ex].
- [54] S. Acharya *et al.* (ALICE), *Phys. Lett. B* **833**, 137272 (2022), arXiv:2104.04427 [nucl-ex].
- [55] S. Acharya *et al.* (ALICE), *Phys. Lett. B* **829**, 137060 (2022), arXiv:2105.05190 [nucl-ex].
- [56] S. Acharya *et al.* (ALICE), *Phys. Lett. B* **844**, 137223 (2023), arXiv:2204.10258 [nucl-ex].
- [57] S. Acharya *et al.* (ALICE), *Phys. Rev. D* **106**, 052010 (2022), arXiv:2201.05352 [nucl-ex].
- [58] S. Acharya *et al.* (ALICE), (2024), arXiv:2401.13541 [nucl-ex].
- [59] (2022), arXiv:2211.02491 [physics.ins-det].
- [60] K. Morita, T. Furumoto, and A. Ohnishi, *Phys. Rev. C* **91**, 024916 (2015), arXiv:1408.6682 [nucl-th].
- [61] K. Morita, A. Ohnishi, F. Etminan, and T. Hatsuda, *Phys. Rev. C* **94**, 031901 (2016), [Erratum: Phys.Rev.C 100, 069902 (2019)], arXiv:1605.06765 [hep-ph].
- [62] A. Ohnishi, K. Morita, K. Miyahara, and T. Hyodo, *Nucl. Phys. A* **954**, 294 (2016), arXiv:1603.05761 [nucl-th].
- [63] J. Haidenbauer, *Nucl. Phys. A* **981**, 1 (2019), arXiv:1808.05049 [hep-ph].
- [64] K. Morita, S. Gongyo, T. Hatsuda, T. Hyodo, Y. Kamiya, and A. Ohnishi, *Phys. Rev. C* **101**, 015201 (2020), arXiv:1908.05414 [nucl-th].
- [65] Y. Kamiya, T. Hyodo, K. Morita, A. Ohnishi, and W. Weise, *Phys. Rev. Lett.* **124**, 132501 (2020), arXiv:1911.01041 [nucl-th].
- [66] K. Ogata, T. Fukui, Y. Kamiya, and A. Ohnishi, *Phys. Rev. C* **103**, 065205 (2021), arXiv:2103.00100 [nucl-th].
- [67] Y. Kamiya, K. Sasaki, T. Fukui, T. Hyodo, K. Morita, K. Ogata, A. Ohnishi, and T. Hatsuda, *Phys. Rev. C* **105**, 014915 (2022), arXiv:2108.09644 [hep-ph].
- [68] J. Haidenbauer and U.-G. Meißner, *Phys. Lett. B* **829**, 137074 (2022), arXiv:2109.11794 [nucl-th].
- [69] Z.-W. Liu, K.-W. Li, and L.-S. Geng, *Chin. Phys. C* **47**, 024108 (2023), arXiv:2201.04997 [hep-ph].
- [70] R. Molina, C.-W. Xiao, W.-H. Liang, and E. Oset, *Phys. Rev. D* **109**, 054002 (2024), arXiv:2310.12593 [hep-ph].
- [71] R. Molina, Z.-W. Liu, L.-S. Geng, and E. Oset, *Eur. Phys. J. C* **84**, 328 (2024), arXiv:2312.11993 [hep-ph].
- [72] V. M. Sarti, A. Feijoo, I. Vidaña, A. Ramos, F. Giacosa, T. Hyodo, and Y. Kamiya, (2023), arXiv:2309.08756 [hep-ph].
- [73] J. Haidenbauer, G. Krein, and T. C. Peixoto, *Eur. Phys. J. A* **56**, 184 (2020), arXiv:2004.08136 [nucl-th].
- [74] Y. Kamiya, T. Hyodo, and A. Ohnishi, *Eur. Phys. J. A* **58**, 131 (2022), arXiv:2203.13814 [hep-ph].
- [75] Z.-W. Liu, J.-X. Lu, and L.-S. Geng, *Phys. Rev. D* **107**, 074019 (2023), arXiv:2302.01046 [hep-ph].
- [76] Z.-W. Liu, J.-X. Lu, M.-Z. Liu, and L.-S. Geng, *Phys. Rev. D* **108**, L031503 (2023), arXiv:2305.19048 [hep-ph].
- [77] I. Vidana, A. Feijoo, M. Albaladejo, J. Nieves, and E. Oset, *Phys. Lett. B* **846**, 138201 (2023), arXiv:2303.06079 [hep-ph].
- [78] N. Ikeno, G. Toledo, and E. Oset, *Phys. Lett. B* **847**, 138281 (2023), arXiv:2305.16431 [hep-ph].
- [79] M. Albaladejo, J. Nieves, and E. Ruiz-Arriola, *Phys. Rev. D* **108**, 014020 (2023), arXiv:2304.03107 [hep-ph].

- [80] J. M. Torres-Rincon, A. Ramos, and L. Tolos, *Phys. Rev. D* **108**, 096008 (2023), arXiv:2307.02102 [hep-ph].
- [81] M. Albaladejo, A. Feijoo, I. Vidaña, J. Nieves, and E. Oset, (2023), arXiv:2307.09873 [hep-ph].
- [82] A. Feijoo, L. R. Dai, L. M. Abreu, and E. Oset, *Phys. Rev. D* **109**, 016014 (2024), arXiv:2309.00444 [hep-ph].
- [83] K. P. Khemchandani, L. M. Abreu, A. Martinez Torres, and F. S. Navarra, (2023), arXiv:2312.11811 [hep-ph].
- [84] H.-P. Li, J.-Y. Yi, C.-W. Xiao, D.-L. Yao, W.-H. Liang, and E. Oset, (2024), arXiv:2401.14302 [hep-ph].
- [85] T. Mehen and J. W. Powell, *Phys. Rev. D* **84**, 114013 (2011), arXiv:1109.3479 [hep-ph].
- [86] M. P. Valderrama, *Phys. Rev. D* **85**, 114037 (2012), arXiv:1204.2400 [hep-ph].
- [87] Q. Wu, M.-Z. Liu, and L.-S. Geng, *Eur. Phys. J. C* **84**, 147 (2024), arXiv:2304.05269 [hep-ph].
- [88] J.-M. Xie, X.-Z. Ling, M.-Z. Liu, and L.-S. Geng, *Eur. Phys. J. C* **82**, 1061 (2022), arXiv:2204.12356 [hep-ph].
- [89] S. E. Koonin, *Phys. Lett. B* **70**, 43 (1977).
- [90] S. Pratt, T. Csörgő, and J. Zimányi, *Phys. Rev. C* **42**, 2646 (1990).
- [91] W. Bauer, C. Gelbke, and S. Pratt, *Annu. Rev. Nucl. Part. Sci.* **42**, 77 (1992).
- [92] D. L. Mihaylov, V. Mantovani Sarti, O. W. Arnold, L. Fabbietti, B. Hohlweger, and A. M. Mathis, *Eur. Phys. J. C* **78**, 394 (2018).
- [93] Y. Kamiya, K. Sasaki, T. Fukui, T. Hyodo, K. Morita, K. Ogata, A. Ohnishi, and T. Hatsuda, *Phys. Rev. C* **105**, 014915 (2022).
- [94] J. Haidenbauer, *Nucl. Phys. A* **981**, 1 (2019).
- [95] O. W. Arnold, *Study of the hyperon-nucleon interaction via femtoscopy in elementary systems with HADES and ALICE*, Ph.D. thesis, Munich, Tech. U. (2017).
- [96] R. L. Workman *et al.* (Particle Data Group), *PTEP* **2022**, 083C01 (2022).

## I. SUPPLEMENTAL MATERIAL

In this Supplemental Material, we apply the theoretical framework proposed in the main manuscript to more general hadron-hadron interactions in the presence of bound, virtual, and resonant states.

### A. CFs corresponding to hadron-hadron interactions in the presence of bound states and comparison with the square model results

In Ref. [75], based on the square-well model, we have revealed some general features of CFs, namely, (1) for a repulsive potential the CF is between zero and unity for different  $R$ , (2) for a weakly attractive potential it is above unity for different  $R$ , (3) for a moderately attractive potential capable of generating a shallow bound state, the low-momentum CF is above unity for a small  $R$  while below unity for a large one, and (4) for a strongly attractive potential that can generate a deep bound state, it remains between zero and unity for sources of all possible  $R$ . The above conclusions can be verified in the framework proposed in this work. The results are shown in Fig. 3. The numerical details are listed in Table II.

TABLE II. Parameters  $a$  ( $b = 0$ ) for a repulsive potential, a weakly attractive potential not strong enough to generate a bound state, a moderately attractive potential capable of generating a shallow bound state, and a strongly attractive potential yielding a deep bound state, respectively. Binding energies  $B$  (in units of MeV), scattering length  $a_0$ , and effective range  $r_{\text{eff}}$  (in units of fm) are also listed. The masses  $m_1$  and  $m_2$  are set at 1800 and 2000 MeV, respectively, and the sharp cutoff  $q_{\text{max}}$  is fixed at 1000 MeV in the calculations.

	$a$	$a_0$	$r_{\text{eff}}$	$B$
Repulsive	100.00	0.13	0.20	...
Weakly attractive	-100.00	-0.57	0.30	...
Moderately attractive	-173.22	3.35	0.28	2.00
Strongly attractive	-247.15	0.88	0.27	40.00

## II. CFS CORRESPONDING TO HADRON-HADRON INTERACTIONS IN THE PRESENCE OF VIRTUAL OR RESONANT STATES—GENERAL FEATURES

In the main manuscript, we have mainly studied the  $D^0 D^{*-} / D^0 D_s^{*-}$  interactions and corresponding CFs. Here, we discuss the findings in a more general setting. In Ref. [75], we have discussed the general features of CFs for attractive interactions of various strengths capable of generating bound states in the square-well model. The conclusions can be verified in the framework proposed in this work, as shown above. The advantage of the present framework is that it can be easily extended to study CFs in the presence of virtual or resonant

states. Here, we mainly focus on whether one can distinguish different interactions in the presence of virtual or resonant states. Without losing generality and focusing on the charm sector, the masses of the two particles  $m_1$  and  $m_2$  are chosen as 1800 and 2000 MeV, close to the masses of  $D$  and  $\bar{D}^*$ . For the resonant state case, the real part of the pole position with respect to the threshold  $\Delta M = M - m_1 - m_2$  is set at 2.5, 5, and 10 MeV, respectively; the imaginary part of the pole position (half-width)  $\Gamma/2$  is set at 1 and 10 MeV, respectively. For the virtual state case,  $\Delta M$  is set at -2.5, -5, and -10 MeV, respectively.

TABLE III. Resonant and virtual state pole positions with respect to the  $m_1 + m_2$  threshold, the values of the parameters  $a$  and  $b$ , the scattering length  $a_0$  and effective range  $r_{\text{eff}}$ . The sharp cutoff  $q_{\text{max}}$  is fixed at 1 GeV.

	$\Delta M + i \Gamma/2$	$a$	$b$	$a_0$	$r_{\text{eff}}$
	[MeV]		[MeV $^{-2}$ ]	[fm]	[fm]
Res.	2.5 + $i$ 1	-108.20	-9234.37	-0.72	-29.43
	5 + $i$ 1	-29.21	-12934.30	-0.07	-570.77
	10 + $i$ 1	195.34	-18219.00	0.18	-17.77
	2.5 + $i$ 10	-127.67	-1260.96	-1.43	-2.62
	5 + $i$ 10	-121.38	-1439.80	-1.12	-3.39
	10 + $i$ 10	-102.39	-1796.48	-0.61	-6.16
Vir.	-2.5	-139.94		0	-2.73
	-5	-133.68		0	-1.89
	-10	-125.38		0	-1.30

The parameters  $a$  and  $b$  required to generate different resonant-state poles, and the corresponding scattering parameters <sup>2</sup> are shown in Table III, and the corresponding CFs are displayed in the left and middle panels of Fig. 4. For a resonant state with a narrow width (left panels), the CF exhibits an enhancement (peak) at momentum slightly below  $k_R$  and a suppression (valley) at momentum slightly above  $k_R$ . However, the peak evolves into an overall enhancement in the low-momentum region for a resonant state with a larger width (middle panels). In contrast, the valley structure in the high-momentum region becomes less pronounced. In addition, the enhancement and suppression weaken as  $k_R$  moves towards the high-momentum region or the source size increases.

For the virtual state case, the detailed information <sup>3</sup> can also be found in Table III, and the corresponding CFs are presented in the right panels of Fig. 4. In this case, the CFs are always

<sup>2</sup> For a resonant state near threshold, the effective range  $r_{\text{eff}}$  is negative, which can be proven by using Eq. (??) and  $k \cot \delta = -1/a_0 + r_{\text{eff}} k^2/2$ .

<sup>3</sup> For a virtual state or a bound state, the effective range  $r_{\text{eff}}$  is positive and small, which is related to the used contact range potential.

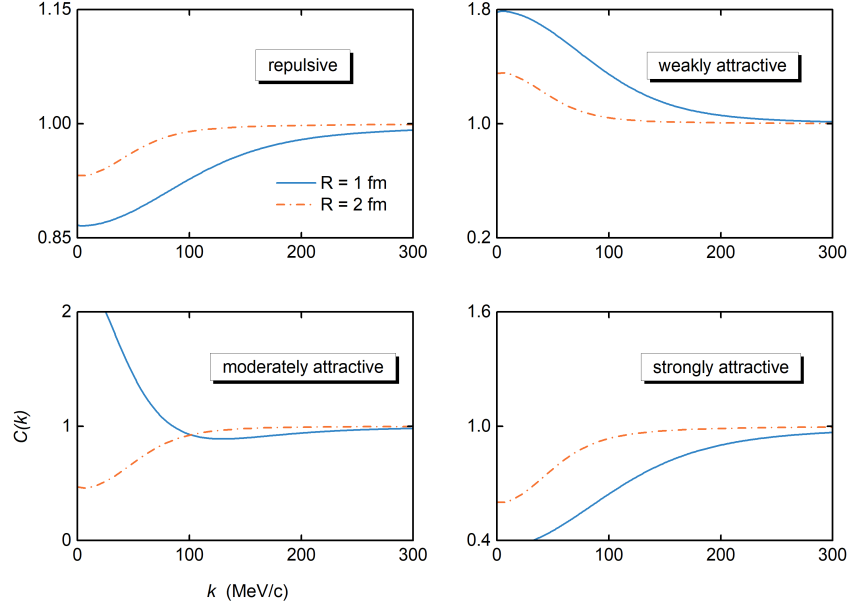


FIG. 3. Correlation functions corresponding to four different potentials: a repulsive potential, a weakly attractive potential, a moderately attractive potential, and a strongly attractive potential. The results are calculated with a source size  $R = 1 \text{ fm}$  (blue solid lines) and  $R = 2 \text{ fm}$  (orange dash-dotted lines).

greater than unity for different source sizes, indicating the existence of a purely attractive interaction. Meanwhile, the attractive strength decreases as the virtual-state pole moves

away from the threshold, reducing the CF. This behavior is consistent with the change of the parameter  $a$  and the scattering length variation with the pole position.

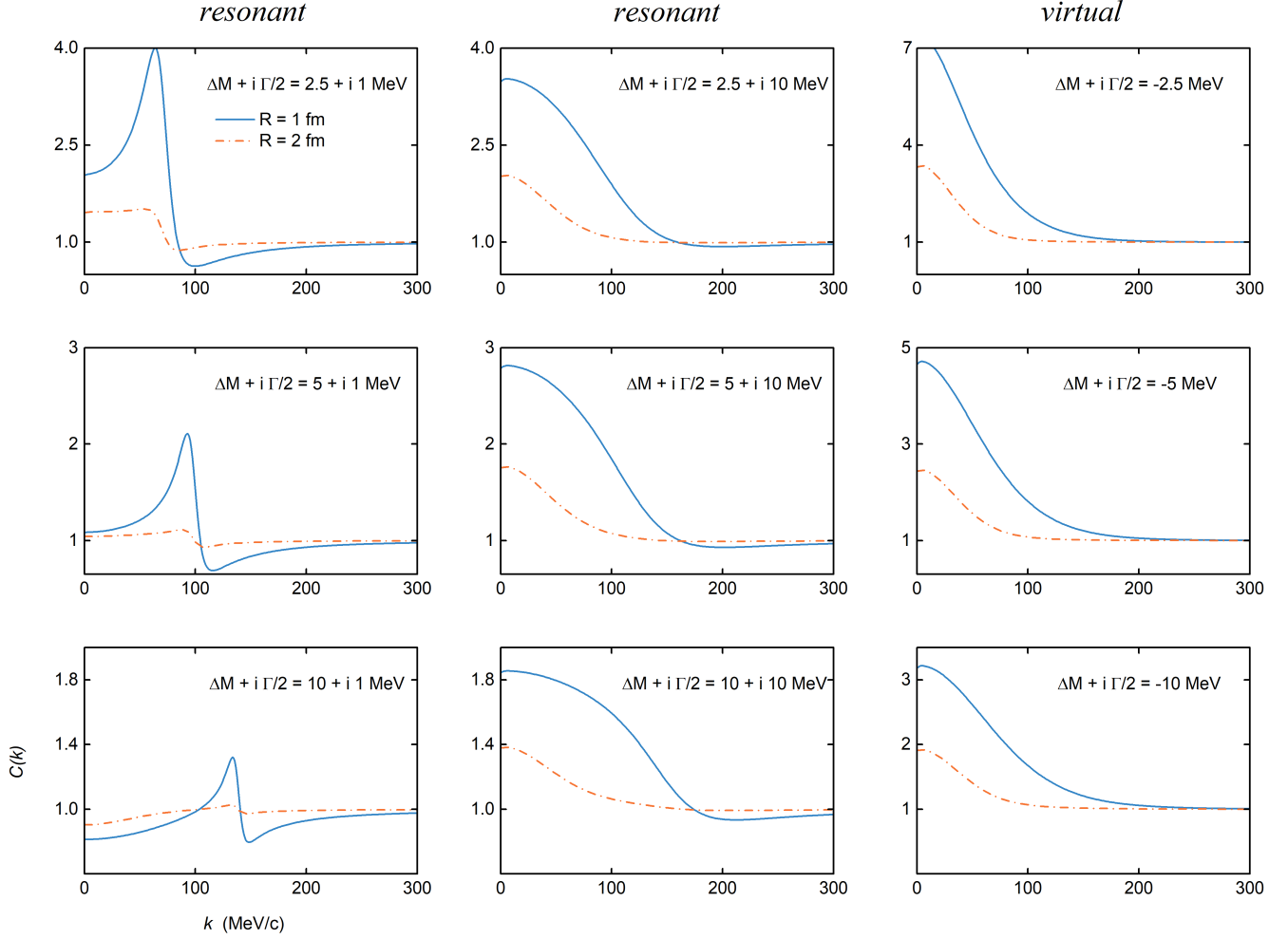


FIG. 4. Correlation functions corresponding to potentials capable of generating a resonant (left and middle panels) or virtual state (right panels) with the pole positions  $\Delta M + i\Gamma/2$  specified in the respective plots. The source sizes are set at  $R = 1$  and 2 fm, and the sharp cutoff  $q_{\max}$  is fixed to 1 GeV.